Biomaterials 31 (2010) 4104–4112

Contents lists available at ScienceDirect

Biomaterials

journal homepage: www.elsevier.com/locate/biomaterials

In situ real-time investigation of cancer cell photothermolysis mediated by excited gold nanorod surface plasmons

Cheng-Lung Chen [a,b,*], Ling-Ru Kuo [c], Ching-Lin Chang [c], Yeu-Kuang Hwu [a], Cheng-Kuang Huang [a], Shin-Yu Lee [a], Kowa Chen [a], Su-Jien Lin [b], Jing-Duan Huang [d], Yang-Yuan Chen [a,**]

[a] *Institute of Physics, Academia Sinica, Taipei, Taiwan, ROC*
[b] *Department of Materials Science and Engineering, National Tsing Hua University, Hsinchu, Taiwan, ROC*
[c] *Department of Physics, Tamkang University, Tamsui, Taiwan, ROC*
[d] *Institute of Marine Biology, National Taiwan Ocean University, Taipei, Taiwan, ROC*

ARTICLE INFO

Article history:
Received 21 December 2009
Accepted 28 January 2010
Available online 23 February 2010

Keywords:
Gold
Plasma
Membrane
Laser
Fluorescence

ABSTRACT

The photothermolysis of living EMT-6 breast tumor cells triggered by gold nanorods (AuNRs) with two-photon irradiation was conducted *in situ* and under real-time observation. The morphology and plasma membrane permeability of the cells were key indicators to the phenomena. AuNRs with an aspect ratio of 3.92, and a longitudinal absorption peak at 800 nm were synthesized with a seed-mediated method. The nanorods surfaces were further modified with polystyrenesulfonate (PSS) for biocompatibility. The prepared nanorods displayed excellent two-photon photoluminescence imaging. *In situ* real-time results revealed cavities internal to the cells were created from thermal explosions triggered by AuNRs localized photothermal effect. The cavitation dynamic is energy dependent and responsible for the perforation or sudden rupture of the plasma membrane. The energy threshold for cell therapy depended significantly on the number of nanorods taken up per cell. For an ingested AuNR cluster quantity $N \sim 10$–30 per cell, it is found that energy fluences E larger-than 93 mJ/cm^2 led to effective cell destruction in the crumbled form within a very short period. As for a lower energy level $E = 18$ mJ/cm^2 with $N \sim 60$–100, a non-instant, but progressive cell deterioration, is observed.

1. Introduction

The application of heat to selectively eliminate or restrain specific cells is a widely acknowledged method in cancer therapy. In general, this non-invasive technique to eradicate tumor cells is referred to as hyperthermia or thermotherapy [1]. Such localized temperature increase can be achieved with a variety of sources, such as radio frequency waves, ultrasound, infrared lamps, alternating magnetic fields and lasers [2]. Once the temperature of the tumor cells reach above 43 °C, protein denaturation together with membrane disruption start to occur inducing cell death [3]. Recently, light-activated therapies on malignant tumor cells have drawn much attention. These methods offer the required localized thermal effect on tumor cells without damaging the surrounding tissues. In this respect, gold nanorod (AuNR) with its good efficacy in converting light energy to heat, is being widely incorporated in biomedical applications [4,5]. AuNRs possess excellent surface plasma resonances in the near infrared that is readily tunable to regions where optical transmission through tissues is at its maximum [6]. While existing results have showed that AuNRs can serve as novel materials for both molecular imaging [7] and photothermal therapy [8,9], open issues remain, in particular, details and mechanisms of the cell destruction process mediated by AuNRs during photothermal therapy.

Photothermal activity of AuNRs is rather beyond simple hyperthermia. Photothermolysis is a more applicable concept [10]; it was used to describe selective heating and localized thermal damage to targeted absorbers. In some respects, cells lysis and necrosis caused by targeted photothermolysis are more reliable; the efficiency depended mostly on laser power and nanorods rather than the properties of specific cells. However, such seemingly simple and lethal technique may originate from a variety of possible pathways. An understanding of the cell destruction process will aid in answering the question as to why certain cells are not susceptible to destruction through photothermolysis.

In this investigation, AuNRs capped with polystyrenesulfonate (PSS–AuNRs) as targeted absorbers were internalized into EMT-6 breast tumor cells. The accumulated PSS–AuNRs clusters in the

* Corresponding author. Institute of Physics, Academia Sinica, Taipei, Taiwan, ROC. Tel.: +886 2 27898301; fax: +886 2 27834187.
** Corresponding author. Tel.: +886 2 27896725; fax: +886 2 27834187.
E-mail addresses: aabbss@phys.sinica.edu.tw (C.-L. Chen), cheny2@phys.sinica.edu.tw (Y.-Y. Chen).

0142-9612/$ – see front matter © 2010 Elsevier Ltd. All rights reserved.
doi:10.1016/j.biomaterials.2010.01.140

cells were then triggered by a two-photon laser with various powers to determine the relation between supplied energy fluences and the degree of cell destruction. Real-time *in situ* observations of the cells were conducted to gain deeper insights into the destruction process. This work presents the photothermolysis of tumor cells prospectively, providing vital information to aiding the improvement of photothermal therapy in clinical trials.

2. Materials and methods

2.1. Synthesis of AuNRs

Gold nanorods were prepared following a reported literature [11]. Briefly, the gold seeds were synthesized by adding $HAuCl_4 \cdot 3H_2O$ (0.5 mM, 2 mL, Chloroauric acid, ACROS) to CTAB (0.2 M, 2 mL, hexadecyltrimethylammonium bromide, Sigma), which were stirred thoroughly. Next, of freshly prepared ice-cold $NaBH_4$ (0.01 M, 240 μL, Sodium borohydride, ACROS) was added to the above solution whilst stirring. The seed solution immediately turned brownish yellow color and was then stirred vigorously for 30 s, then gently stirred for further 15 min at 40–45 °C to ensure removal of excess $NaBH_4$. The prepared seeds were stored at 27 °C, and used within 1–3 h. After that, the nanorod growth solution was prepared by adding $HAuCl_4 \cdot 3H_2O$ (1 mM, 15 mL) into CTAB (0.2 M, 15 mL) and stirred thoroughly. Next, the growth solution was added with $AgNO_3$ (0.004 M, Silver Nitrate, ACROS) depending on the aspect ratio required; typically, adding ~750 μL will produce nanorods with aspect ratio about 4. After thoroughly stirring the solution, ascorbic acid (0.788 M, 220 μL, ACROS) was slowly added into the solution, and after this application, the solution should be transparent. Then, 38 μL of gold seed was quickly added to the solution, and stirred vigorously for 20 s. After this the samples were gently stirred for about 2 h till completion. The solution should start changing color within 10 min or so. Upon completion, the rods were centrifuged at 14000 rpm for 5 min and re-dispersed in deionized water. For further characterizations, the UV–visible absorption spectra of AuNRs were obtained by the spectrophotometer (Spectronic, GENESYS-8). Meanwhile, the sizes and aspect ratios of nanorods were determined by the field emission transmission electron microscope operated at 200 kV (JEOL, JEM-2100). The concentration of the nanorods could be estimated from the experimental absorbance and its correlated extinction coefficients [12].

2.2. Surface modification with polystyrenesulfonate

A CTAB-AuNRs suspension (6 mL, O.D. ~ 1) was centrifuged at 14000 rpm for 6 min and re-dispersed in 3 mL deionized water. The prepared PSS solution (10 mg/mL in 1 mM NaCl solution, 70 kDa, Aldrich) was added into the nanorods solution in a 1:1 volume ratio and allowed to react for 1 day. The nanorods were then collected by centrifugation at 7000 rpm for 30 min, and resuspended in a NaCl (1 mM) solution, the resulting solution was further reacted with another aliquot PSS solution for 1 day. The above procedure was repeated at least three times, and the final PSS–AuNRs suspension was purified using an ultrafiltration cell (Millipore, Millex-GP).

2.3. Cell culture and incubation with PSS–AuNRs

EMT-6 breast tumor cells are transplantable murine mammary tumor cell lines that have been exploited extensively as a model to study the effects of various treatments on local tumor growth and pulmonary metastasis. The cell cultures were maintained in humidified air containing 5% CO_2 at 37 °C. The medium involved 1% penicillin–streptomycin (Invitrogen) and 10% fetal bovine serum (FBS, invitrogen). When the cell confluence was about 80%, PSS–AuNRs suspensions were added to cultured wells at optimal concentrations. The cell incubations were performed at the same environment overnight. Before any assay described here are conducted, all cells were washed with PBS to remove excess nanorods and placed in fresh solutions which contained YOPRO-1 and propidium iodide dyes (Molecular Probes OR, USA).

2.4. Cell viability assay (MTT)

Colorimetric assay is a popular method in quantifying cell survival percentage [13]. In principle, the absorbance of formazan which was produced from the mitochondrial oxidation of 3-(4,5-dimethylthiazolyl-2)-2,5-diphenyltetrazolium bromide (MTT) in living cells is directly proportional to the number of living cells. Briefly, EMT-6 cells were planted into 96-well plates with 300 μL medium and incubated at 37 °C under a 5% CO_2 atmosphere for 24 h. After that, these cells were further incubated for 24 and 48 h with CTAB- and PSS-coated AuNRs respectively at varying concentrations, then treated with a freshly prepared 12 mM MTT solution (10 μL) and incubated for an additional 3 h. Next, the MTT solutions were removed and 50 μL DMSO (Dimethylsulfoxide, Sigma) was added to each well. The wells were left for half an hour in the dark, and then assayed with an automated reader, fixing the absorbance at 570 nm. The obtained cell viability was expressed as a percentage relative to cells incubated with medium only.

2.5. Two-photon luminescence imaging and photothermolysis

The *in vitro* two-photon imaging and photothermolysis were carried out on an inverted scanning microscope (LSM510, META/Observer, Z1, Zeiss). A femtosecond (fs) Ti:Sapphire laser (Spectra-physics MaiTai HP) with a duration time of 100 fs and a repetition rate of 80 MHz was used as the excitation source. The wavelength and average power of the laser beam were tunable, and a water-immersion objective lens (NA = 1.4) was used. For AuNRs excitations, the wavelength was fixed at 790 nm. Typically, an area of 90 μm × 90 μm (512 pixels × 512 pixels) was scanned at a rate of 1.57 s for imaging, thereby the exposure time per pixel per scan is 5.98 μs (each pixel area = 176 × 176 nm^2). For photothermolysis mediated by AuNRs, a relatively slow exposure time of 163.83 μs per pixel per scan was applied to activate PSS–AuNRs. The exposure time of AuNRs was calculated following known methods [8]. Briefly, the focal spot area was calculated as $\pi d^2/4$, where d is the full width at half maximum of the beam waist, and was calculated from the formula, $d = 0.61\,\lambda/\mathrm{NA}$. In such condition, the total exposure time for nanorods was estimated to (focal spot area/pixel area) × 163.83 μs = 504.60 μs per scan. In this work, one scan of five different excited power densities (222, 185, 111, 55, and 37 W/cm^2) was applied to the specimens. The energy fluence was calculated from the product of power density and the total exposure time. The following are their corresponding energy fluences, 113, 93, 56, 28, and 18 mJ/cm^2, respectively.

2.6. Preparation of cell specimens for electron microscopy

The EMT-6 cells were cultured on cover slides for 48 h, and then fixed by immersing in a fixative solution (2.5% glutaraldehyde and 3% paraformaldehyde in 0.1 M PBS) at 4 °C for 24 h. After pre-fixation, cover slides were washed in 0.1 M PBS, and post-fixed in 1% osmium tetroxide (OsO_4) solutions for 1 h, and washed in 0.1 M PBS again. After these procedures, cover slides with EMT-6 cells were dehydrated in ethanol series, and then placed into a critical-point dryer (Hitachi, HCP-2) for critical-point drying. Finally, the specimens were pasted onto aluminum stubs and coated with gold/palladium alloy by an ion sputter (Hitachi, E101) for observation by a scanning electron microscope (SEM, Hitachi, S-4200). For transmission electron micrographs, the EMT-6 cells were cultured in a Petri dish for 72 h and then detached from the Petri dish by trypsin treatment. Next, they were transferred to a fixative solution for several hours and pelleted by centrifugation at 1000 rpm for 5 min. These cell pellets were soaked in pre-fixative solution again for 1 h, and washed in 0.1 M PBS. Then, cell pellets were post-fixed in OsO_4 solution for 1 h, and washed in 0.1 M PBS. Subsequently cells were dehydrated in ethanol series and acetone. Samples were infiltrated in Spurr's embedding mediums with different proportions of acetone in order and finally transferred into pure Spurr's medium in the capsules, then placed at 70 °C for about 14 h to harden. The ultrathin sections were cut to 70–100 nm by using an ultramicrotome (LEICA, EM, UC6), and stained with uranyl acetate ($UO_2(CH_3COO)_2.2H_2O$) and lead citrate ($Pb(C_6H_2O_7)_2.3H_2O$) for observation by a transmission electron microscope (TEM, Hitachi, H-600).

3. Results

3.1. Cytotoxicity studies of AuNRs

The AuNRs were prepared by the typical seed-mediated growth method using hexadecyltrimethylammonium bromide (CTAB) as surfactants, CTAB–AuNRs [11]. Fig. 1a shows a typical TEM image of as-prepared AuNRs capped with CTAB. The statistically averaged aspect ratio is 3.92 ± 0.26. However, the surfactants with poor biocompatibility, due to its cytotoxicity [14], were demonstrated to be a problem in application. In order to make AuNRs suitable for imaging and adopting as theranostic agents for clinical purposes, additional surface modifications are imperative. On reviewing recent literatures pertaining to AuNRs, polyelectrolyte-coated AuNRs were found to be the best candidate, exhibiting excellent dispersion stability and biocompatibility. Polystyrenesulfonate sodium salt (PSS, 70 kDa) was, therefore, chosen as a peptizing agent and detergent for the efficient removal of CTAB from AuNRs suspensions [15]. This scalable modification produces AuNRs having easy dispersion control. The PSS–AuNRs are presented in the schematic cartoon in the inset of Fig. 1b. From Fig. 1b, it is seen that the longitudinal plasmon band of CTAB-capped AuNRs peak at 800 nm, and is slightly shifted to 790 nm after PSS substitution. The produced water-soluble PSS–AuNRs are extremely stable at room temperature for several months.

In order to maximize the contribution of collateral photothermal damage caused by subsequent near IR laser shinning, it is

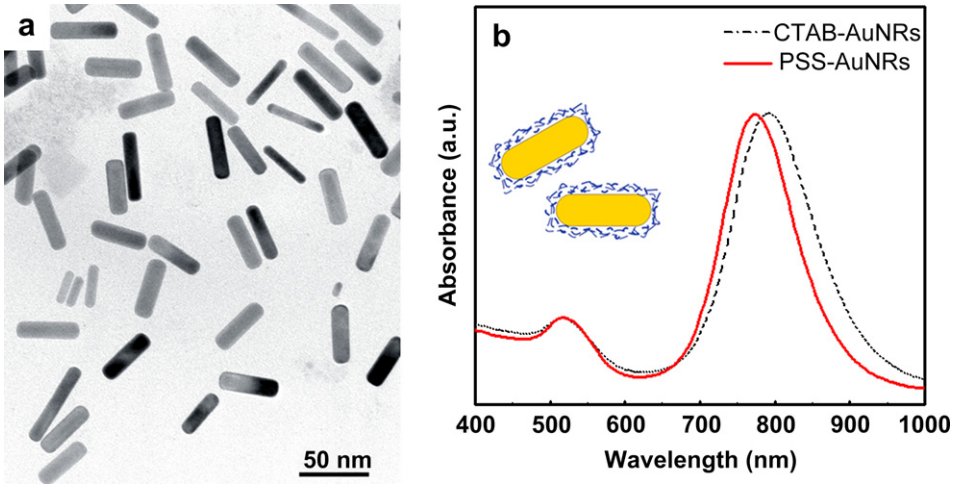

Fig. 1. (a) TEM micrograph of Au nanorods. (b) Absorption spectroscopy of CTAB–AuNRs and PSS–AuNRs. Inset: The schematic diagram of PSS–AuNRs.

vital to exclude side effects arising from the capping agents. The cytotoxicity of the AuNR related samples was evaluated against EMT-6 breast tumor cells, using a standard colorimetric cell viability assay (MTT assay), as shown in Fig. 2. The detailed protocol for MTT assay can be found elsewhere [13]. The assay evidently verified that CTAB–AuNRs presented conspicuous cytotoxicity after incubation with the cells for 24 and 48 h. Even at low concentration of 0.8 μg/mL, the cell viability was less than 18% after 48 h incubation. In comparison, the viability of cells with PSS–AuNRs, was as high as 80%, confirming its biocompatibility with EMT-6 cells, and can thus be used in further studies pertaining to *in vitro*/*in vivo* imaging and photothermal therapeutics.

3.2. Two-photon photoluminescence imaging of AuNRs in tumor cells

The characteristics of two-photon photoluminescence (TPPL) of PSS-AuNRs clusters can be confirmed by the nonlinear dependence of photoluminescence intensity on excitation power [16,17]. Briefly describing, the PSS–AuNRs were dispersedly deposited on a cover slide, and photoluminescence from a single spot was examined. As shown in Fig. 3a, a quadratic dependence of emission intensity on the input power was obtained, indicating the evidence of two-photon excitation. Fig. 3b shows typical TPPL imaging of PSS–AuNRs in cells. The excellent surface plasma resonance of PSS–AuNRs in the near IR region makes them ideal probes for TPPL imaging of cells. During imaging, a total of eight "z slices" is taken, moving from the bottom of the cell to the top, mapping the distribution of PSS–AuNRs clusters in the cells. The acquired data were processed by 3D visualization software, and presented at the margin plots in Fig. 3b. At the same time, the ingested AuNR cluster quantity *N* could be estimated for further quantitative analysis. Obviously, PSS–AuNRs appeared inside the cells, and not just settling on the plasma membrane. This fact can also be confirmed by staining plasma membrane with Alexa Fluor 350 (Molecular Probes OR, USA). Fig. 3c shows the cellular profiles clearly presented in blue, while the pink spots revealed the locations of AuNRs clusters inside cellular cytoplasm.

The cellular uptake of AuNRs was realized through endocytosis which is a fast and general process, delivering clusters of nanorods or small particles from the cell membrane into the cytoplasm. In general, the ingested nanorods will eventually reside in lysosomes (final degrading organelles) within several hours of incubation. Briefly, AuNRs are first internalized by cells through endocytosis and trapped in endosomes. These endosomes then fuse with lysosomes for processing prior to being transported to the cell

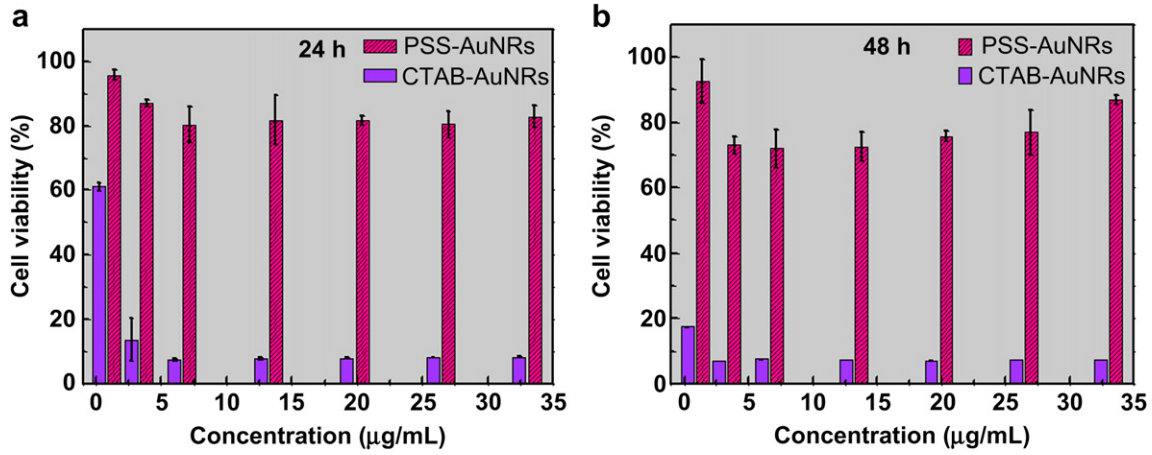

Fig. 2. Cell viability of EMT-6 cells exposed to CTAB- and PSS-coated AuNRs after (a) 24 and (b) 48 h incubation, respectively. The viability of the cells was normalized with respect to a media-only control.

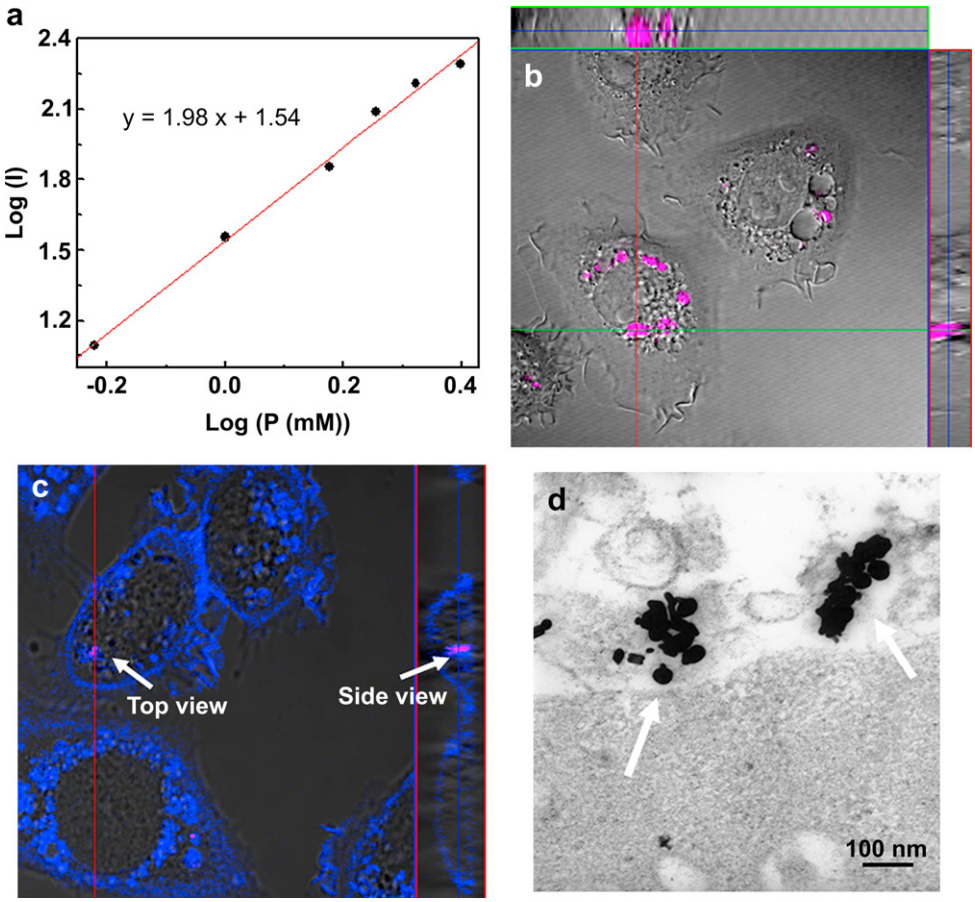

Fig. 3. (a) Dependence of photoluminescence intensity on the excitation power of clusters of AuNRs. (b) Visualization of the tumor cells labeled by PSS–AuNRs. The top and right margin plots in figure clearly display the cross-section view of the cell. The crucifix composed of green and red lines are guidelines for look. (c) Plasma membrane staining with Alexa Fluor 350 (blue); the pink spots were the locations of AuNRs clusters. (d) TEM micrograph of PSS–AuNRs inside EMT-6 cells.

periphery for excretion. In other words, they are localized either in endosomes or lysosomes [18,19]. The TEM imaging in Fig. 3d demonstrates that AuNRs are subsequently accumulated at internal vacuoles. The ingested quantities of nanorods in each cluster are roughly estimated to about 30–100 from the TEM images. On average, a few hundred to thousands of nanorods were taken up per cell. It is worth noting that this normal biological process will congregate nanorods into larger clusters inside endosomes or lysosomes. We believe this is beneficial to the reduction of energy fluence threshold in photothermolysis. The details are discussed in the following section.

3.3. *In situ real-time observation of selective photothermolysis in tumor cells*

In this work, the destruction of tumor cells triggered by PSS–AuNRs assisted with two-photon laser excitation was continuously monitored using fluorescent dyes exclusion method [20]. In principle, as cell destruction initiates, its plasma membrane will begin to become permeable, which will allow fluorescent dyes outside the cell to gradually flow into the nucleus. The most common dyes used for this purpose are those incorporated in nucleic acid labeling, which are YOPRO-1 (green coloring) and propidium iodide (red coloring). These two dyes have the following characteristics and are thus suited to our dynamic monitoring. As the cell membrane becomes slightly permeable, it will enable YOPRO-1 but not propidium iodide to enter the cytoplasm. However, upon cell death, propidium iodide can penetrate the comparatively leaky membranes. Neither of two dyes can penetrate viable cells. This method, in effect, act as a qualitative indicator of the cells plasma membrane integrity.

To understand the influence of different energy fluences on the destruction of cancer cells, five different energy fluences were applied to living cells in sequence. The corresponding morphologies and fluorescent color variations in the nucleus and its vicinity were monitored *in situ* under real-time. Details of energy fluence calculation can be found in the experimental section. It is worth noting that in the absence of AuNRs, the cells could still survive under the excited energy fluence of 93 mJ/cm^2, however, cell mortality was observed at 113 mJ/cm^2 energy fluence. This result is consistent with the established safety standard for medical lasers (100 mJ/cm^2) [21]. Results of the cells with AuNRs ($N \sim$ 10–30 clusters), under excitation at energy fluences of 113 and 93 mJ/cm^2, are shown in the series of images in Fig. 4; the images were taken within a period of 60 s. Upon reaching an energy fluence of 113 mJ/cm^2 (over safety standard), the whole cell would be seriously destroyed through bombardment (Fig. 4a–d). As for the energy fluence of 93 mJ/cm^2, somewhat lower than the safety standard, a discernible internal explosion phenomenon occurred upon excitation (Fig. 4e–h). Meanwhile, the formation of characteristic cavities (shadows indicated by arrows) was especially pronounced at AuNRs cluster locations (cluster size: 2–3 μm). The diameter of the cavities can reach as large as 10 μm. Such cavitation dynamics is recognized to be responsible for the transient micro-bubbles

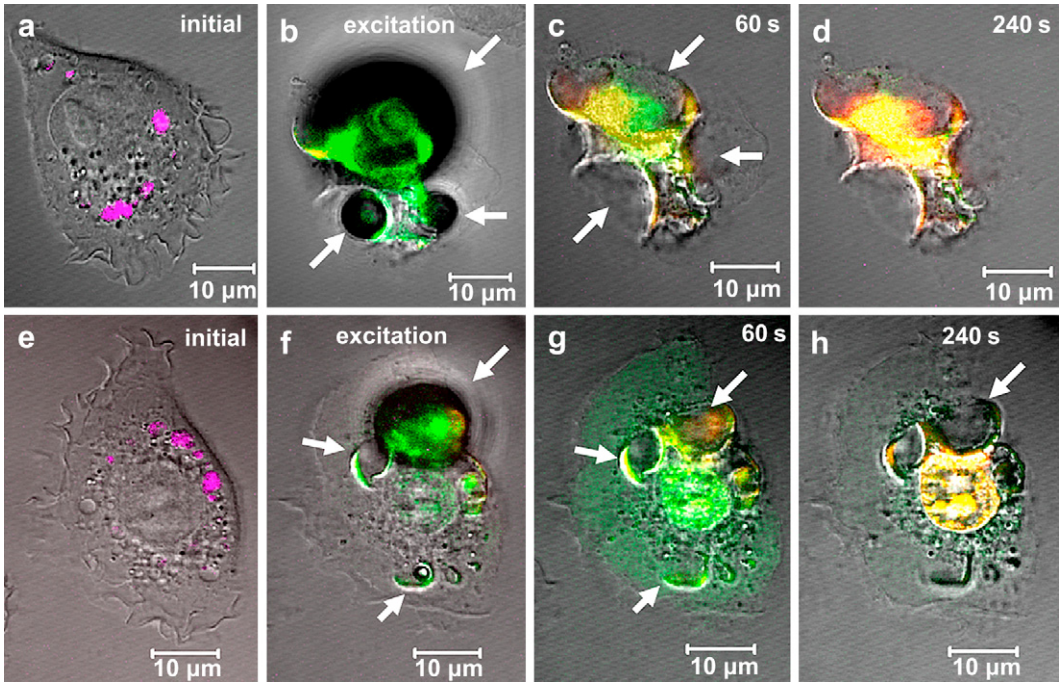

Fig. 4. Photothermolysis of the EMT-6 tumor cell triggered by AuNRs under different energy fluences. (a–d) 113 mJ/cm^2; (e–h) 93 mJ/cm^2.

formation, and causes the perforation or sudden rupture on plasma membrane [22]. Death of the targeted cells, with symptoms of oncosis, occurred promptly within 4 min. This can be identified from dual-color staining of the nucleus and its vicinity; owing to the leaky membrane of the necrotic cell, thus allowing both of YOPRO-1 and propidium iodide to infiltrate. The TPPL signals at the irradiated sites also quickly diminished after the explosions. Such incapability to resonate under irradiation implies that most of the AuNRs may have melted. Lowering the energy fluence to 56 mJ/cm^2, shown in Fig. 5, the internal explosions were more moderate than those caused by higher energy levels. As energy fluence was reduced to 28 mJ/cm^2, the explosion phenomena were still observable; however, the total time for the cell transiting to necrosis was relatively longer, around 960 s, shown in Fig. 6. Intuitively, the lesions of plasma membrane arising from different energy fluences should be different and led to dissimilar destruction of cells. Confirming this, a scanning electron microscope was also utilized to visualize the differences of surface morphologies of the post-irradiated cells in three dimensions. Under control conditions, cells without AuNRs subjected to 93 mJ/cm^2 stayed alive. They are characteristic of a spread out flattened morphology, and are attached to the slides (Fig. 7a). Fig. 7b and c show the

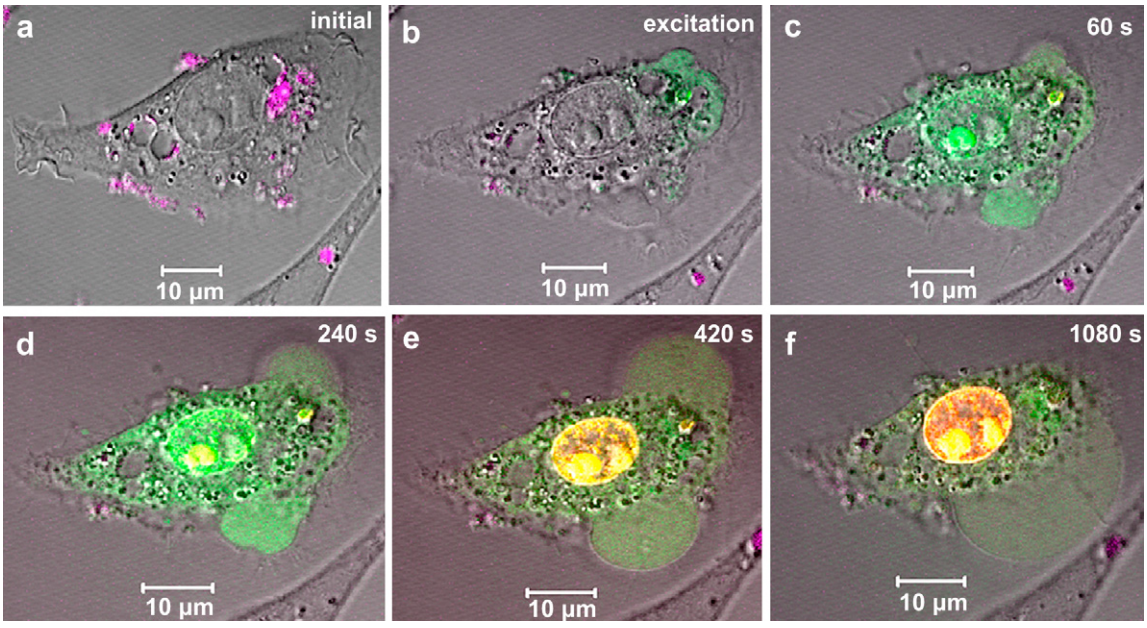

Fig. 5. Photothermolysis of the EMT-6 tumor cell triggered by AuNRs under the energy fluence of 56 mJ/cm^2.

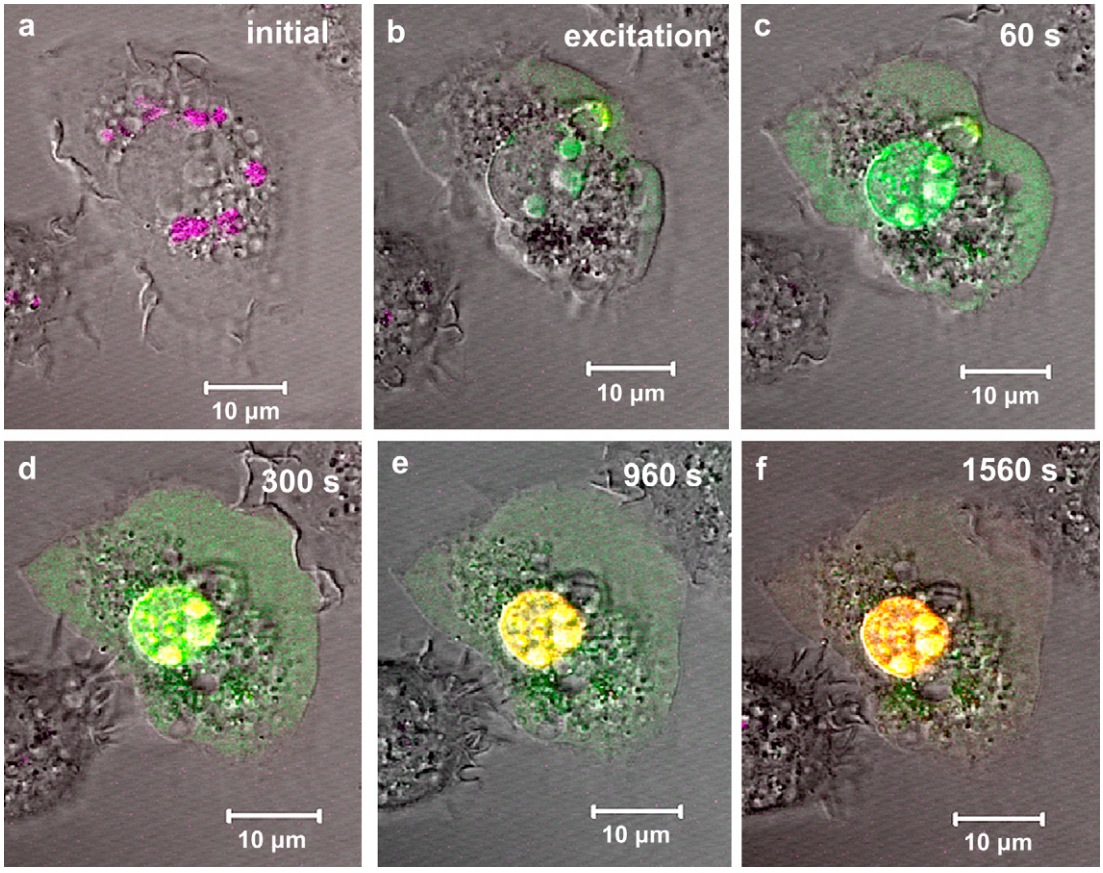

Fig. 6. Photothermolysis of the EMT-6 tumor cell triggered by AuNRs under the energy fluence of 28 mJ/cm^2.

morphologies of the cells ingested with AuNRs under different energy fluence excitation. For 93 mJ/cm^2, the cell seemed to be pulverized by the nanorods. In contrast, for 28 mJ/cm^2, only a few cavities with fissures were found on the irregular surface of the cell.

Further lowering the energy fluence, to 18 mJ/cm^2, the explosion phenomena and its resulting vanishing TPPL were still apparent, however, the cells survived the trauma (Fig. 8a–c). It was noticed that as the ingested cluster numbers of AuNRs are relatively high as 60–100 (Fig. 8d), the energy fluence of 18 mJ/cm^2 was still effective in damaging the tumor cells. From Fig. 8d–i, all the fluorescence from AuNRs clusters disappeared at the moment of excitation. Green fluorescence (at nucleus district) was not easily observable by the naked eyes prior to 240 s, but morphological changes of the cell were identifiable with a distinctive swelling, blebbing and deformation, and led to a hydropic appearance before the cyto-architecture collapses. At 540 s, the YOPRO-1 dye completely stained the nucleus region and revealed the discernible green coloring, whereas propidium iodide was still excluded out of the plasma membrane. As time went on, the cell nucleus began to display green and yellow mingled color, and finally showing a wholly bright orange color at 2880 s. At this point, the cell was dead and was regarded as irreversible post-mortem remains.

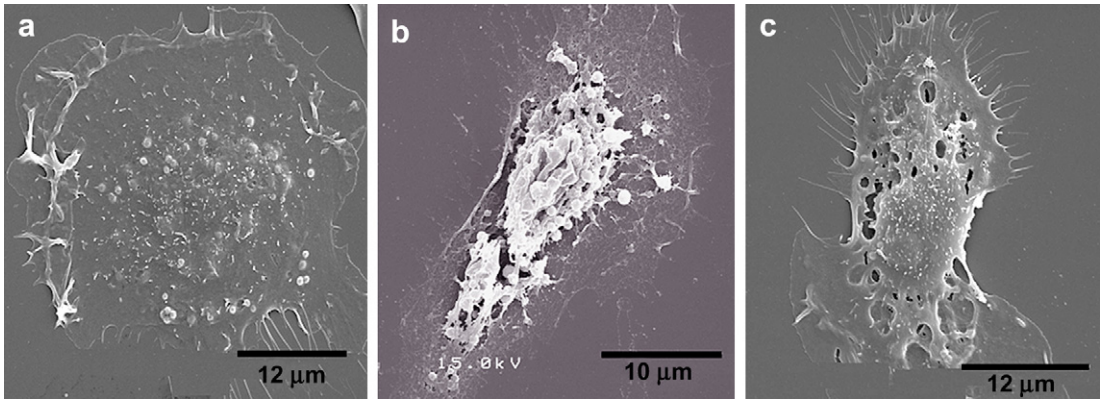

Fig. 7. Scanning electron micrographs of EMT-6 cells after laser excitation. (a) 93 mJ/cm^2, cells without AuNRs. (b) 93 mJ/cm^2, cells incubated with AuNRs. (c) 28 mJ/cm^2, cells incubated with AuNRs.

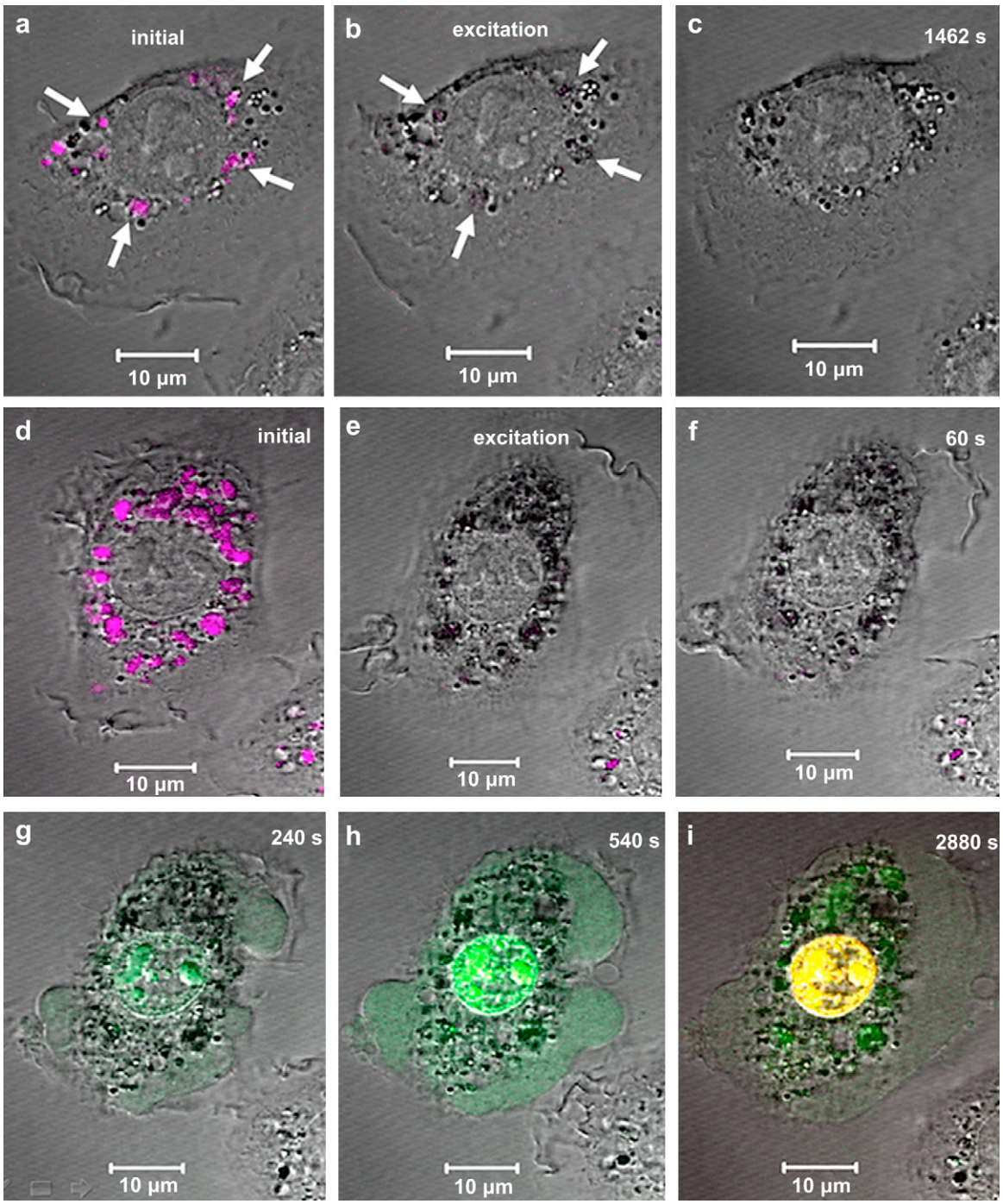

Fig. 8. Photothermolysis of the EMT-6 tumor cell triggered by AuNRs under energy fluence of 18 mJ/cm^2 (a–c) Uptake number of AuNRs clusters was few. (d–i) Uptake number of AuNRs clusters was relative high.

Accordingly, the uptake quantities of AuNRs by cells were crucial to lowering energy threshold for effective destruction.

4. Discussion

Our investigation has revealed that AuNRs mediated photothermal effect is different from conventional hyperthermia techniques, in which the temperature of the whole of the selected tumor cells was raised above the cell-killing threshold margin. According to dynamic monitoring results, we propose that AuNRs can serve as "nano-bomb" agents that function to destroy intracellular organs or metabolism processes through micro-explosions within the cells. This concept is based on the unique property of AuNRs; surface plasmons are excited upon irradiation with short laser pulses corresponding to the collective excitation wavelength of the surface electrons; 800 nm along the longitudinal direction in this investigation. In time these plasmons may decay by re-radiation, and/or diminish by effective electron-phonon conversion of the acquired photon energy into thermal energy through rapidrelaxation (picoseconds time scale). Once the temperature of

the AuNRs is rather higher than liquid vaporization temperature (~150–350 °C), melting point (~1063 °C), or even boiling point (~2710 °C), thermal explosion is realized when heat is generated more rapidly than it can diffuse away [23]. The accompanied sudden local heating or shock waves may fatally crack the vital cellular components, even the outer membrane.

It has been observed that cell destruction greatly depend on the energy fluence. In the case of higher energy fluence (higher power density) excitation, it was undoubted that the cells died completely in the crumbled form within a very short time. In such situations, the amount of AuNRs within a cell influences insignificantly. In contrast, as the cells were treated with near lowest energy fluence of 18 mJ/cm^2, and with a higher population of AuNRs, the morphology and fluorescent dyes exclusion indicate that such intracellular explosions did not damage the plasma membrane immediately. The follow-up intracellular complex responses should crucially determine whether the plasma membrane remains intact or broken-down. Herein, we have showed that the ingested AuNRs finally almost all resided in lysosomes, thus the above-mentioned intracellular explosions greatly affected lysosomes rupture. One group suggested that the level of lysosomal rupture could greatly affect the cell destruction [24]. Since the release of hydrolytic enzymes from ruptured lysosomes could cause an increase in the total volume of acidic compartments (VAC; constituted mostly by lysosomes) within the cell, which was demonstrated to be a key factor in plasma membrane disruption. Considering also, the prevalent assumption that apoptosis could be initiated by reparable damage of lysosomes, but cell lysis (necrosis) always resulted from a sudden mass destruction of lysosomes. We thus speculate that the observed non-instant but progressive damages triggered by AuNRs in EMT-6 tumor cells may involve such argument. During the micro-explosions, lysosomes within the cell would suffer from a sudden mass destruction, owing to their pronounced rupture susceptibility. Hence the severity of the damage is beyond self-repair, thus the greater chance in inducing plasma membrane disruption. Further more, the cell destruction process was initiated with oncosis, not apoptosis, accompanied by cellular swelling, blebbing and increased membrane permeability, finally resulting in necrosis. Though, the blebbing response was attributed to an influx of extracellular calcium ions into the cytoplasm [8]. An increase in intracellular calcium concentration was also found to be a trigger of lysosomal exocytosis in L929 and MCF-7 cells [25,26]. Through this, calcium ions may be contributing towards expediting necrosis. Contemplating previous facts, the cell destruction resulting from AuNRs triggered photothermolysis is intimately linked with cavitation dynamics.

The uptake amounts of NRs in cells also played an important role in terms of AuNRs-based photothermolysis. In Fig. 8a–c, although the energy fluence of 18 mJ/cm^2 could bring about small-scale explosions within the cells, the damages were probably not severe enough to bring about unrepairable injuries to cells. This result could elucidate that why certain cells were not susceptible to photothermolysis induced destructions. Therefore, highly targeting AuNRs are truly imperative to photothermal therapy, offering greater efficiency within the safety criterion. Exploring the potentials further, the researches on functionalization of AuNRs for specific binding to tumor cells are in progress.

5. Conclusions

In summary, highly stabilized PSS–AuNRs were prepared and exhibited excellent two-photon photoluminescence imaging. The cytotoxicity assay was performed to exclude other possible influences towards cell viability, thus showing photothermal effect as the dominant cell-killing factor. The destruction process was studied *in situ* under real-time observation by progressive dual-color fluorescent staining of the nucleus and its vicinity. The results showed that localized photothermal effect of AuNRs was large enough to trigger a considerable explosion, resulting in cavities inside cells. The cavitation dynamic is energy dependent and responsible for the perforation or sudden rupture of the plasma membrane. It is also found that larger energy fluence (higher power density) leads to effective cell death within a very short time. On the contrary, a non-instant but progressive destruction process was observed for lower energy level. The mechanism of the phenomenon was discussed. Accordingly, the energy threshold for cell therapy, significantly dependent on the amount of nanorods taken up per cell, and was much lower than the medical safety level. These results provide useful insight towards evaluating and improving the performance of AuNRs-based photothermal therapy.

Acknowledgements

This work was supported by the National Research Council of the Republic of China under Grant No. NSC 97-2120-M-001-007. We thank Dr. Chi-Keung Chan for his help with UV–visible absorption spectra analysis, and Ms. Shu-Chen Shen for her help with two-photon imaging analysis.

Appendix

Figures with essential color discrimination. All figures in this article are difficult to interpret in black and white. The full color images can be found in the on-line version, at doi:10.1016/j.biomaterials.2010.01.140.

References

[1] Wust P, Hildebrandt B, Sreenivasa G, Rau B, Gellermann J, Riess H, et al. Hyperthermia in combined treatment of cancer. Lancet Oncol 2002;3:487–97.
[2] Quesson B, de Zwart JA, Moonen CTW. Magnetic resonance temperature imaging for guidance of thermotherapy. J Magn Reson Imaging 2000;12:525–33.
[3] Dewey WC. Arrhenius relationships from the molecule and cell to the clinic. Int J Hyperthermia 1994;10:457–83.
[4] Chou CH, Chen CD, Wang CRC. Highly efficient, wavelength-tunable, gold nanoparticle based optothermal nanoconvertors. J Phys Chem B 2005;109:11135–8.
[5] Huang X, El-Sayed IH, Qian W, El-Sayed MA. Cancer cell imaging and photothermal therapy in the near-infrared region by using gold nanorods. J Am Chem Soc 2006;128:2115–20.
[6] Weissleder R. A clearer vision for in vivo imaging. Nat Biotechnol 2001;19:316–7.
[7] Durr NJ, Larson T, Smith DK, Korgel BA, Sokolov K, Ben-Yakar A. Two-photon luminescence imaging of cancer cells using molecularly targeted gold nanorods. Nano Lett 2007;7:941–5.
[8] Tong L, Zhao Y, Huff TB, Hansen MN, Wei A, Cheng JX. Gold nanorods mediate tumor cell death by compromising membrane integrity. Adv Mater 2007;19:3136–41.
[9] Li JL, Day D, Gu M. Ultra-low energy threshold for cancer photothermal therapy using transferrin-conjugated gold nanorods. Adv Mater 2008;20:3866–71.
[10] Anderson RR, Margolis RJ, Watenabe S, Flotte T, Hruza GJ, Dover JS. Selective photothermolysis of cutaneous pigmentation by Q-switched Nd-YAG laser-pulses at 1064, 532, and 355 nm. J Invest Dermatol 1989;93:28–32.
[11] Nikoobakht B, El-Sayed MA. Preparation and growth mechanism of gold nanorods (NRs) using seed-mediated growth method. Chem Mater 2003;15:1957–62.
[12] Orendorff CJ, Murphy CJ. Quantitation of metal content in the silver-assisted growth of gold nanorods. J Phys Chem B 2006;110:3990–4.
[13] Mosmann T. Rapid colorimetric assay for cellular growth and survival: application to proliferation and cytotoxicity assays. J Immunol Methods 1983;65:55–63.
[14] Takahashi H, Niidome Y, Niidome T, Kaneko K, Kawasaki H, Yamada S. Modification of gold nanorods using phospatidylcholine to reduce cytotoxicity. Langmuir 2006;22:2–5.
[15] Leonov AP, Zheng J, Clogston JD, Stern ST, Patri AK, Wei A. Detoxification of gold nanorods by treatment with polystyrenesulfonate. ACS Nano 2008;2:2481–8.

[16] Bouhelier A, Bachelot R, Lerondel G, Kostcheev S, Royer P, Wiederrecht GP. Surface plasmon characteristics of tunable photoluminescence in single gold nanorods. Phys Rev Lett 2005;95:267405–8.
[17] Wang HF, Huff TB, Zweifel DA, He W, Low PS, Wei A, et al. In vitro and in vivo two-photon luminescence imaging of single gold nanorods. Proc Natl Acad Sci U S A 2005;102:15752–6.
[18] Chithrani BD, Stewart J, Allen C, Jaffray DA. Intracellular uptake, transport, and processing of nanostructures in cancer cells. Nanomedicine 2009;5:118–27.
[19] Lewinski N, Colvin V, Drezek R. Cytotoxicity of nanoparticles. Small 2008;4:26–49.
[20] Wronski R, Golob N, Grygar E, Windisch M. Two-color, fluorescence-based microplate assay for apoptosis detection. Biotechniques 2002;32:666–8.
[21] American national standard for safe use of lasers ANSI Z136.1. Orlando, Florida: American Laser Institute; 2000.
[22] Lapotko DO, Lukianova E, Oraevsky AA. Selective laser nano-thermolysis of human leukemia cells with microbubbles generated around clusters of gold nanoparticles. Lasers Surg Med 2006;38:631–42.
[23] Letfullin RR, Joenathan C, George TF, Zharov VP. Laser-induced explosion of gold nanoparticles: potential role for nanophotothermolysis of cancer. Nanomedicine 2006;1:473–80.
[24] Ono K, Kim SO, Han J. Susceptibility of lysosomes to rupture is a determinant for plasma membrane disruption in tumor necrosis factor alpha-induced cell death. Mol Cell Biol 2003;23:665–76.
[25] Ono K, Wang X, Han J. Resistance to tumor necrosis factor-induced cell death mediated by PMCA4 deficiency. Mol Cell Biol 2001;21:8276–88.
[26] Rodriguez A, Webster P, Ortego J, Andrews NW. Lysosomes behave as Ca^{2+}-regulated exocytic vesicles in fibroblasts and epithelial cells. J Cell Biol 1997;137:93–104.